Supplementary Information

Selective CO_2 electroreduction to formate over Cu-based catalyst in S^{2-}-containing electrolyte

Shuyu Liang[1,2,#], Ziyi Fang[1,2,#], Chaoran Yang[1,2,], Qiang Wang[1,2,*]

[1]College of Environmental Science and Engineering, Beijing Forestry University, Beijing 100083, China

[2]State Key Laboratory of Efficient Production of Forest Resources, Beijing Forestry University, Beijing 100083, China

[#]Equal contribution

[*]Email: qiangwang@bjfu.edu.cn (Q. Wang)

Experimental Section

Materials

Copper chloride dihydrate ($CuCl_2 \cdot 2H_2O$, 99.99%), ascorbic acid($C_6H_8O_6$, 99%), potassium sulfide (K_2S, 99%), and formic acid (HCOOH, 99%) were purchased from Aladdin Reagent Co., Ltd. (Shanghai, China). Sodium hydroxide (NaOH, 96%), potassium bicarbonate ($KHCO_3$, 99.7%), potassium hydroxide (KOH, 85%), and anhydroelectric ethanol (C_2H_5OH, 99.99%) were purchased from Beijing Innokai Technology Co., LTD. (Beijing, China). Nafion (5%) is purchased from Shanghai Sanshik Industrial Co., Ltd. (Shanghai, China).

Synthesis of Cu_2O

Cu_2O nanocube was synthesized by a previously reported ligand-free method with slight modification. 10 mL of 0.1 M $CuCl_2 \cdot 2H_2O$ solution was added to 400 mL of deionized water, then 30 mL of 0.2 M NaOH solution was added to the solution to form a blue flocculent precipitate. After stirring for 5 min, 20 mL of 0.1 M ascorbic acid solution was added dropwise to the solution described above and further stirred for 1 hour. The solution was then washed several times with ethanol and water and finally dried in a vacuum oven.

For the catalyst ink preparation, 5 mg of the as-prepared catalyst was mixed with 1.0 mL ethanol and 20 μL 5 wt.% Nafion solution, and then ultrasonicated for at least 30 min. Then, 56 μL of the ink was slowly drop-casted on the glassy carbon electrode with a diameter of 6 mm to obtain a catalyst loading of 1 mg cm^{-2}.

Characterizations

The morphology of the samples were characterized by field emission scanning electron microscopy (FESEM, SU8010) and transmission electron microscopy (TEM, FEI Talos F200S, operated at 200 kV). High-angle annular dark field scanning transmission electron microscopy (HAADF-STEM) and energy dispersive X-ray spectroscopy (EDX) were carried out on a FEI Talos F200S microscope. The crystal structure of the catalysts was analyzed by X-ray diffraction (XRD, Shimadzu-7000) equipped with Cu Kα radiation. The surface composition of the samples was determined by X-ray photoelectron spectroscopy (XPS, Thermo Scientific ESCALAB 250Xi). All spectra of the sample were calibrated to the C 1s binding energy at 284.8 eV. XPS depth profiles were obtained by etching using an Ar ion beam.

Electrochemical measurements and product analysis

The electrochemical measurements were performed in a commercial H-type cell separated by a Nafion 117 membrane. A Pt mesh and an Ag/AgCl electrode were used as the counter electrode and the reference electrode, respectively. The linear sweep voltammetry (LSV) tests were performed in CO_2-saturated 0.1 M $KHCO_3$ electrolyte containing different concentrations of K_2S (0, 0.01, 0.05, 0.25 mM) at a scan rate of 20 mV s^{-1} in a potential range from 0 to –2.0 V vs. RHE. Constant electrolysis was performed at the potential window from –1.0 to –1.4 V vs. RHE (no IR correction) in the H-type cell.

The flow cell is composed of three chambers: gas, catholyte and anolyte chambers. The catalyst ink was dropped onto a gas diffusion layer (GDL, AvCarb GDS2230) with a catalyst loading of 0.5 mg cm^{-2} to obtain the gas diffusion electrode (GDE). The

Ag/AgCl and Pt foil were used as the reference electrode and anode, respectively. A Nafion 117 membrane was employed to separate the catholyte from the anolyte chamber. In the flow cell, 1 M KOH was selected as electrolyte and a series of amounts of 50 mM K_2S was added to reach the concentration of 0.00, 0.05, 0.25, 1.00 and 2.50 mM. CO_2 was flowed into the gas chamber behind the GDE at a rate of 20 mL min^{-1}, and it can diffuse through the gas diffusion electrode to the surface of the catalyst and form a three-phase interface with the electrolyte. Constant electrolysis was performed at the current density window from –50 to –200 mA cm^{-2} in the flow cell.

The gas products were quantified by online gas chromatography (Shimadzu GC-2014C). A thermal conductivity detector (TCD) was employed to determine H_2, and a flame ionization detector (FID) was used to determine CO, CH_4 and C_2H_4. The liquid product of formic acid/formate was determined by High-Performance Liquid Chromatography (HPLC, Shimadzu). The Faradaic efficiency (FE) was calculated through Eq. (1), where Q_{total} is the total charge passed during electrolysis (C), N_i is the number of moles for the target product (mol), n is the number of electrons transferred (e.g., 2 for CO), and F is the Faraday constant (96485 C mol^{-1}).

$$FE = \frac{N_i \times n \times F}{Q_{total}} \times 100\% \quad (1)$$

Fig. S1. The HAADF-STEM image and the corresponding energy dispersive X-ray spectroscopy (EDX) elemental mappings of Cu_2O.

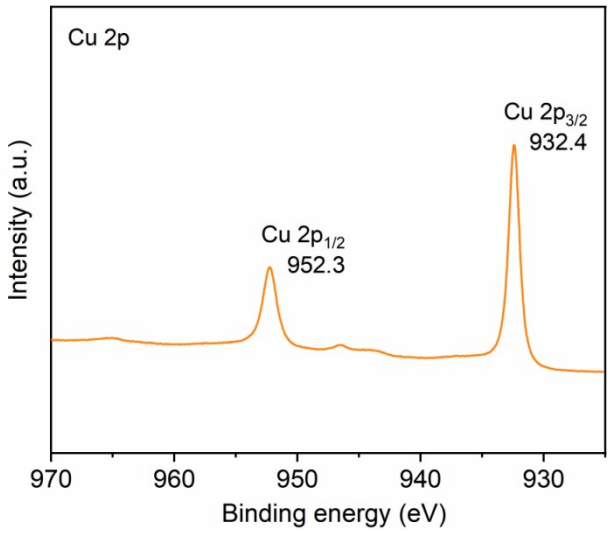

Fig. S2. Cu 2p XPS spectrum of Cu_2O.

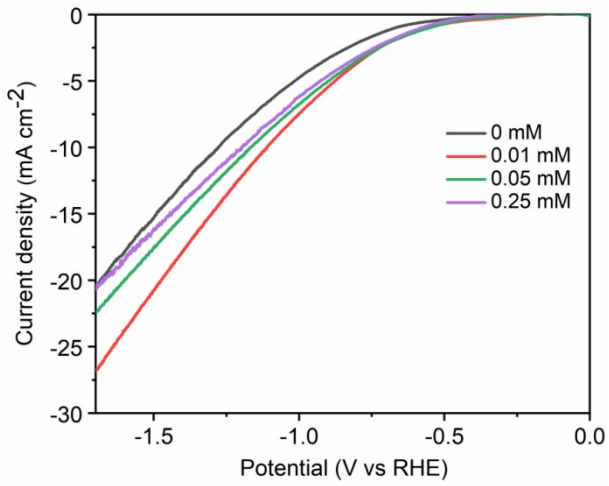

Fig. S3. LSV curves of Cu_2O in CO_2-saturated electrolytes containing different concentrations of K_2S.

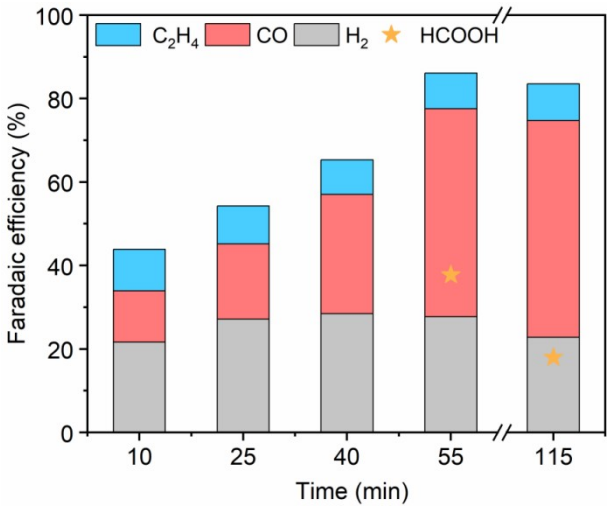

Fig. S4. The products' FE of Cu_2O/Cu_xS along with the reaction time.

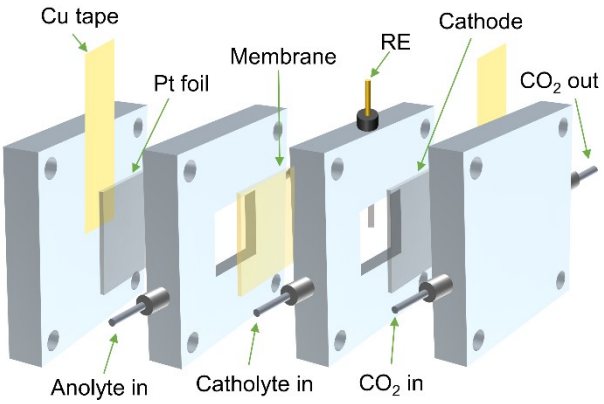

Fig. S5. Schematic illustration of the flow cell configuration.

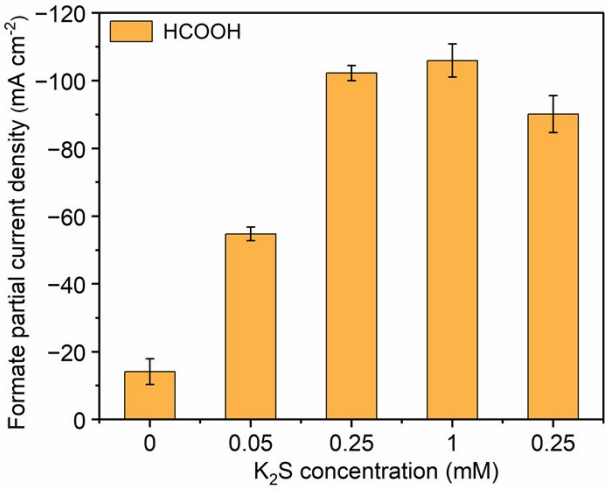

Fig. S6. Formate partial current density for Cu_2O catalysts in electrolytes containing different concentrations of K_2S at -150 mA cm^{-2}.

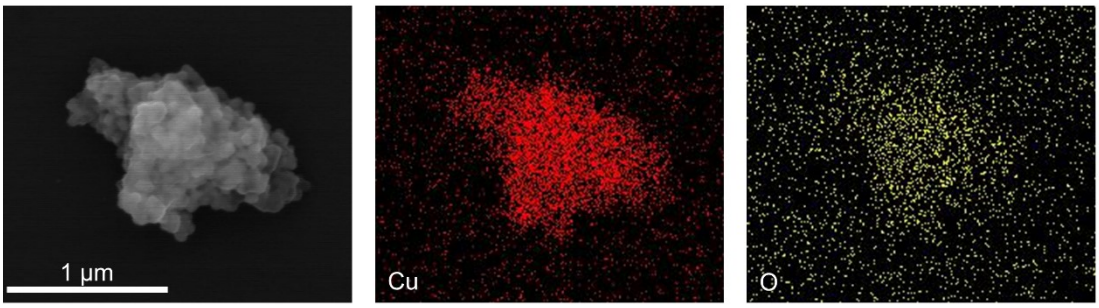

Fig. S7. The SEM image and the corresponding energy dispersive X-ray spectroscopy (EDX) elemental mappings of Cu_2O after CO_2 RR.

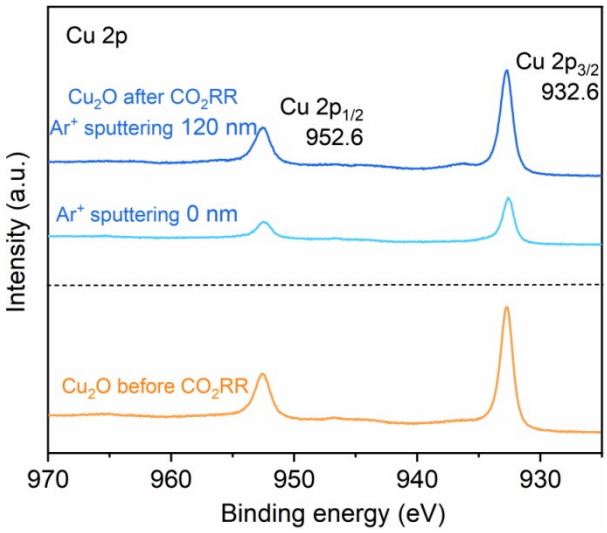

Fig. S8. Cu 2p XPS spectrum of Cu_2O before and after CO_2RR in the electrolyte containing K_2S.

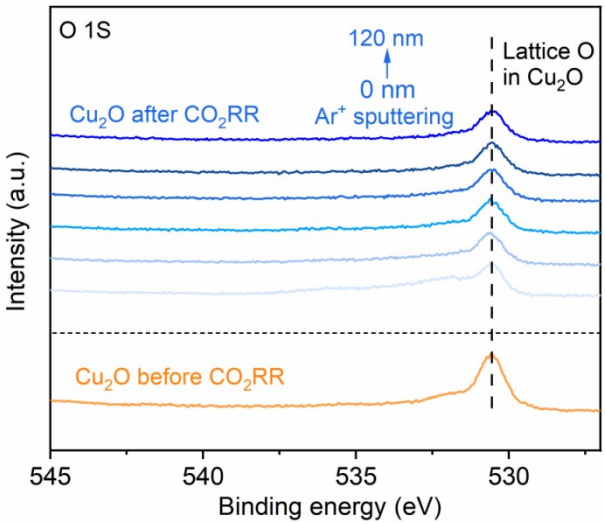

Fig. S9. O 1s spectrum of Cu_2O before and after CO_2RR in the electrolyte containing K_2S.

Table. S1. Performance comparison of Cu-based catalysts for CO_2 electroreduction to formate.

Catalyst	Electrolyte	Potential V vs. RHE	$J_{formate}$ (mA cm^{-2})	Formate FE (%)
Cu_2O (H-type cell) This work	0.1 M $KHCO_3$+ 0.05 mM K_2S	−1.2	8.3	74
Cu_2O (Flow cell) This work	1 M KOH+1 mM K_2S	/	105.9	70.6
Commercial Cu_2S[1]	0.1 M $KHCO_3$	−0.86	~3.6	~36
CuS[2]	0.1 M $KHCO_3$	−0.6	1.5	98 (keep decreasing from 98% to 40% during 8 h)
5% PTFE Cu array[3]	0.1 M $KHCO_3$	−0.7	2.3	41
Cu_2S NSs/C[4] (H-type cell)	0.1 M $KHCO_3$	−1.2	8.9	71.4
Cu_2S NSs/C[4] (Flow cell)	0.1 M $KHCO_3$	/	205	82
S-doped Cu/Cu foil[5]	0.1 M $KHCO_3$	−0.8	10.7	75
CuS 811 (H-type cell)[6]	0.1 M $KHCO_3$	−1.0	~7.5	92
CuS 811 (flow cell)[6]	1 M KOH	/	172	86
Cu_2O/CuS[7]	0.1 M $KHCO_3$	−0.9 V	15.3	67.6
S3-Cu_2O-70[8]	0.1 M $KHCO_3$	−0.9 V	260 (flow cell)	90
Cu nanoflower[9]	0.1 M $KHCO_3$	−1.6	9	50
CuS/N,S-rGO[10]	0.5 M $KHCO_3$	−0.63	~4.8	82
AC-CuS_x[11]	0.1 M $KHCO_3$	−0.9	9	75
L-S CuS_x[12]	0.1 M $KHCO_3$	−0.9	~10	80
CuS/BM[13]	0.5 M $KHCO_3$	−0.7	75	67.8

Reference

1 L. Liang, L. Yang, T. Heine, A. Arinchtein, X. Wang, J. Hübner, J. Schmidt, A. Thomas and P. Strasser, *Advanced Energy Materials,* 2024, **14**.

2 M. Wang, X. Li, X. Ma, J. Wang, X. Jin, L. Zhang and J. Shi, *ChemSusChem,* 2023, **16**, e202300879.

3 Z. Cai, Y. Zhang, Y. Zhao, Y. Wu, W. Xu, X. Wen, Y. Zhong, Y. Zhang, W. Liu, H. Wang, Y. Kuang and X. Sun, *Nano Res.,* 2018, **12**, 345-349.

4 W. Liu, Y. Wen, N. Fang, M. Wang, Y. Xu and X. Huang, *Chem Commun (Camb),* 2023, **59**, 11843-11846.

5 Y. Huang, Y. Deng, A. D. Handoko, G. K. L. Goh and B. S. Yeo, *ChemSusChem,* 2018, **11**, 320-326.

6 Y. Wang, H. Xu, Y. Liu, J. Jang, X. Qiu, E. P. Delmo, Q. Zhao, P. Gao and M. Shao, *Angew. Chem., Int. Ed.,* 2024, **63**, e202313858.

7 S. Wang, T. Kou, J. B. Varley, S. A. Akhade, S. E. Weitzner, S. E. Baker, E. B. Duoss and Y. Li, *ACS Mater. Lett.,* 2020, **3**, 100-109.

8 X. Ma, Y. Zhang, T. Fan, D. Wei, Z. Huang, Z. Zhang, Z. Zhang, Y. Dong, Q. Hong, Z. Chen and X. Yi, *Adv. Funct. Mater.,* 2023, **33**, 2213145.

9 J.-F. Xie, Y.-X. Huang, W.-W. Li, X.-N. Song, L. Xiong and H.-Q. Yu, *Electrochimica Acta,* 2014, **139**, 137-144.

10 Z. Wu, J. Yu, K. Wu, J. Song, H. Gao, H. Shen, X. Xia, W. Lei and Q. Hao, *Appl. Surf. Sci.,* 2022, **575**, 151796.

11 L. Mandal, K. R. Yang, M. R. Motapothula, D. Ren, P. Lobaccaro, A. Patra, M. Sherburne, V. S. Batista, B. S. Yeo, J. W. Ager, J. Martin and T. Venkatesan, *ACS Appl. Mater. Interfaces,* 2018, **10**, 8574-8584.

12 T. Shinagawa, G. O. Larrazábal, A. J. Martín, F. Krumeich and J. Pérez-Ramírez, *ACS Catal.,* 2018, **8**, 837-844.

13 T. Dou, Y. Qin, F. Zhang and X. Lei, *ACS Appl. Energy Mater.,* 2021, **4**, 4376-4384.